Metabolic impact of heterologous protein production in *Pseudomonas putida*: Insights into carbon and energy flux control

Philippe Vogeleer[1], Pierre Millard[1,2], Ana-Sofia Ortega Arbulú[4], Katharina Pflüger-Grau[4], Andreas Kremling[4] and Fabien Létisse[1,3]*

[1]Toulouse Biotechnology Institute, Université de Toulouse, INSA, UPS, Toulouse, France.

[2]MetaToul-MetaboHUB, National Infrastructure of Metabolomics and Fluxomics, Toulouse, France.

[3]Present address: Institut de Pharmacologie et de Biologie Structurale (IPBS), Université de Toulouse, CNRS, Université Toulouse III - Paul Sabatier (UT3), Toulouse, France

[4]Technical University Munich, TUM School of Engineering and Design, Department of Energy and Process Engineering, Systems Biotechnology, Germany

***Corresponding author**

Fabien Létisse : fabien.letisse@univ-tlse3.fr

Abstract

For engineered microorganisms, the production of heterologous proteins that are often useless to host cells represents a burden on resources, which have to be shared with normal cellular processes. Within a certain metabolic leeway, this competitive process has no impact on growth. However, once this leeway, or free capacity, is fully utilized, the extra load becomes a metabolic burden that inhibits cellular processes and triggers a broad cellular response, reducing cell growth and often hindering the production of heterologous proteins.

In this study, we sought to characterize the metabolic rearrangements occurring in the central metabolism of *Pseudomonas putida* at different levels of metabolic load. To this end, we constructed a *P. putida* KT2440 strain that expressed two genes encoding fluorescent proteins, one in the genome under constitutive expression to monitor the free capacity, and the other on an inducible plasmid to probe heterologous protein production. We found that metabolic fluxes are considerably reshuffled, especially at the level of periplasmic pathways, as soon as the metabolic load exceeds the free capacity. Heterologous protein production leads to the decoupling of anabolism and catabolism, resulting in large excess energy production relative to the requirements of protein biosynthesis. Finally, heterologous protein production was found to exert a stronger control on carbon fluxes than on energy fluxes, indicating that the flexible nature of *P. putida*'s central metabolic network is solicited to sustain energy production.

Highlights : (3 – 5 bullet points/85 characters)

Heterologous protein production in *P. putida* reshuffles the periplasmic metabolism.

Increased protein production progressively decouples catabolism from anabolism.

Protein production exerts a stronger control on energy than on carbon fluxes.

Glucose is directed towards ATP production to meet the elevated energy demands.

Keywords: Heterologous protein production, *P. putida*, fluxomics, metabolic control, metabolic burden, resource allocation

43 **1. Introduction**

44 *Pseudomonas putida* is widely regarded as a valuable workhorse for white biotechnology due
45 to its combination of rapid growth, minimal nutrient requirements, and versatile metabolism
46 (Nikel and de Lorenzo, 2018). Its resistance to toxic compounds, organic solvents and to
47 variations in pH and temperature also make it attractive for industrial applications. Moreover,
48 *P. putida* lacks the virulence factors commonly found in the genome of other *Pseudomonas*
49 species (*i.e.* type III secretion system and endotoxin A) (Udaondo et al., 2016). Its ability to
50 produce endogenous biopolymers (polyhydroxyalkanoates - PHA), biosurfactants
51 (rhamnolipids) and bioplastic synthon (2,5-furandicarboxylic acid - FDCA) is already
52 industrially exploited (Weimer et al., 2020). It is also used in bioremediation processes, as it
53 produces various enzymes that degrade xenobiotic aromatic compounds (de Lorenzo, 2008;
54 Poblete-Castro et al., 2017). This ability to degrade aromatic compounds and its high intrinsic
55 resistance to metabolic and physiological stresses differentiates *P. putida* from other bacterial
56 species used in synthetic biology such as *Escherichia coli* and *Bacillus subtilis* (Nikel et al.,
57 2014), and makes *P. putida* a promising organism for biotechnological applications.

58 However, biotechnological production is often limited by cellular capacity (Ceroni et al., 2015)
59 and in engineered cells, the heterologous production of proteins represents an unnatural load,
60 which consumes energy and cellular resources, such as ribosomes, polymerases and
61 metabolites. Cells have a certain metabolic leeway, which we call their *free capacity*, that
62 allows them to produce heterologous proteins without reducing their growth rate. Any
63 additional load, however, becomes a burden and the growth rate decreases (Borkowski et al.,
64 2016). The central metabolism responds by providing precursors, and chemical and redox

65 energy for the implemented task, but this also triggers stress-induced mechanisms related to
66 protein production (Wittmann et al., 2007).

67 *P. putida*'s metabolism is characterized by its particular central carbon network (Figure 1). At
68 the periplasmic level, glucose is primarily directly oxidized to gluconate with a smaller fraction
69 being converted to 2-ketogluconate (2-KG). Once internalized into the cytoplasm by their
70 respective transporters, these metabolites are converted into 6-phosphogluconate (6-PG)
71 either by gluconate kinase (GntK) or *via* the 2-KG bypass, by the activity of 2-KG kinase (KguK)
72 and 2-KG-6-P reductase (KguD) (del Castillo et al., 2007; Vicente and Cánovas, 1973).
73 Furthermore, the classical Embden–Meyerhof–Parnas (EMP) pathway is nonfunctional
74 because of the absence of phosphofructokinase, which normally converts fructose-6-
75 phosphate to fructose-1,6-biP. As a consequence, carbon is processed mainly *via* the Entner-
76 Doudoroff (ED) pathway and partially *via* the pentose phosphate (PP) pathway (Nikel et al.,
77 2015). Compared to the EMP pathway, commonly known as glycolysis, the oxidation of one
78 mole of glucose into two pyruvates through the ED pathway yields less ATP (one mole only)
79 but an equal amount of catabolic and anabolic reducing power (one NADH and one NADPH
80 molecule, respectively) instead of two NADHs. Remarkably, NADPH formation is also boosted
81 by the recycling of the glyceraldehyde-3-phosphate (GAP) formed from glucose in the ED
82 pathway to hexose-phosphate, and the combined action of enzymes from the ED pathway,
83 the EMP pathway (in the gluconeogenic direction) and the PP pathway, in what is collectively
84 known as the EDEMP cycle (Kohlstedt and Wittmann, 2019; Nikel et al., 2015). The EDEMP
85 cycle enables *P. putida* to adjust NADPH production to meet anabolic demands and provides
86 the intrinsic resistance to oxidative stress (Kim and Park, 2014). The cyclic architecture of *P.*
87 *putida*'s metabolism thus supports stress resistance alongside oxidative energy production. In
88 the context of biotechnology applications (Volke et al., 2020), an important question is how

89 the specific features of *P. putida*'s central metabolism allow the bacteria to cope with the
90 metabolic load incurred by protein overproduction.

91 The aim of this study was to characterize the rearrangements in *P. putida*'s central metabolism
92 at different levels of protein overproduction. Following Ceroni *et al*. (2015), we constructed a
93 *P. putida* KT2440 strain that i) constitutively expressed the *mCherry* gene to monitor cellular
94 capacity and ii) carried a plasmid encoding maltose-binding protein (MBP) fused to fluorescent
95 eGFP for better detection under the control of an inducible promoter. Protein production was
96 tuned by varying the concentrations of the inducer, and quantified by measuring the level of
97 green fluorescence. The metabolic response to the different levels of metabolic burden
98 induced by gradually increasing heterologous protein production was investigated by
99 measuring bacterial growth and carbon and energy fluxes. Comparisons between metabolic
100 flux maps obtained under induced and non-induced conditions provide insights into the flux
101 rearrangements within the central metabolism caused by protein production.

102 **2. Material and Methods**

103 **2.1 Strains and plasmids**

104 *P. putida* and *E. coli* strains were cultivated at 30 °C and 37 °C, respectively, in either LB or M9
105 minimal medium (Miller, 1972) with glucose as C-source. Strains were stored in cryotubes at
106 -80 °C, in LB medium containing 15 % glycerol (v/v).

107 ***Construction of the capacity monitor strain, P. putida CAP.*** *P. putida* CAP was constructed by
108 inserting the *mCherry* gene into the chromosome of *P. putida* KT2440 under the control of a
109 constitutive promoter. The promoter of the *lac*-operon of *E. coli* was chosen, as this promoter
110 is only regulated by its genomic context (Oehler, 2009). The fragment containing the *mCherry*

111 gene under the control of *lacIp* was cloned into pTn7-M (Zobel et al., 2015) choosing SpeI and
112 SacI restriction sites in *E. coli* DH5α λpir. The resulting pTn7-M_lacIp-*mCherry* vector was
113 introduced into *P. putida* KT2440 by four-parental mating with *E. coli* DH5α λpir (pTn7-
114 M_lacIp-*mCherry*) as donor, *E. coli* HB101 (pRK600) as a helper strain for conjugation, *E. coli*
115 DH5α (pTnS1) to provide transposase, and *P. putida* KT2440 as recipient (Choi and Schweizer,
116 2006; Zobel et al., 2015). The resulting *P. putida* KT2440 *attTn7::lacIp-mCherry* strain, referred
117 to as *P. putida* CAP (for capacity), was selected by growth on citrate and resistance towards
118 gentamycin. The correct integration of *lacIp-mCherry* was confirmed by amplification of a
119 fragment spanning the *lacIp-mCherry* region and sequencing.

120 ***Construction of the burden plasmid pSEVA438-MBPeGFP*.** The *malE* gene was genetically
121 fused *via* a GlySer-linker (GGGGS) to the N-terminus of *eGFP* by overlap extension PCR.
122 Primers were designed to remove the periplasmic signal sequence of *malE* to avoid
123 extracellular transport of the heterologous protein. eGFP was tagged on the C-terminus with
124 a polyhistidine-tag (6xHis-tag), yielding the MBPeGFP fragment. The fragment was ligated into
125 pSEVA438 using EcoRI and SpeI as restriction sites and the resulting plasmid, pSEVA438-
126 MBPeGFP, was transferred to *E. coli* DH5α λpir using the TSS method (Chung et al., 1989).
127 Positive clones were then selected by streptomycin resistance. After verification of
128 pSEVA438_MBPeGFP by sequencing, the plasmid was transferred to *P. putida* CAP by
129 triparental mating (de Lorenzo and Timmis, 1994), yielding *P. putida* CAP
130 (pSEVA438_MBPeGFP) (Figure 2A).

131 **2.2 Media and preculture conditions.** For each experiment, the strains were first streaked
132 onto LB agar plates containing 200 µg/mL streptomycin and incubated overnight at 30 °C.
133 Then, 3 mL of LB medium with 200 µg/mL streptomycin were inoculated from a single isolated

134 colony and the cultures were incubated for 8 to 16 h at 30 °C and 200 rpm in an orbital shaker
135 (Inova 4230, New Brunswick Scientific, New Brunswick, NJ, USA). Cells were first diluted
136 (1/100) in 50 mL of M9 medium containing 17.4 g ·L^{-1} $Na_2HPO_4 \cdot 12H_2O$, 3.0 g·L^{-1} KH_2PO_4, 2.0
137 g.·L^{-1} NH_4Cl, 0.5 g.L^{-1} NaCl, 0.5 g·L^{-1} $MgSO_4$, and 3.3 mg·L^{-1} $CaCl_2$, and 1 mL of a trace element
138 solution containing 15 mg·L^{-1} $Na_2EDTA \cdot 2H_2O$, 4.5 mg·L^{-1} $ZnSO_4 \cdot 7H_2O$, 0.3 mg·L^{-1} $CoCl_2 \cdot 6H_2O$,
139 1 mg·L^{-1} $MnCl_2 \cdot 4H_2O$, 1 mg·L^{-1} H_3BO_3, 0.4 mg·L^{-1} $Na_2MoO \cdot 2H_2O$, 3 mg·L^{-1} $FeSO_4 \cdot 7H_2O$, 0.3
140 mg·L^{-1} $CuSO_4 \cdot 5H_2O$. M9 preculture medium was supplemented with 3 g·L^{-1} glucose for flux
141 analysis, or with 3 g·L^{-1} of a glucose mixture containing 80 % $^{13}C_1$-labeled glucose and 20 % U-
142 $^{13}C_6$-labeled glucose (Eurisotop, Saint Aubin, France). The glucose, $MgSO_4$ and trace element
143 solutions were sterilized by filtration (Minisart 0.2-μm syringe filter; Sartorius, Göttingen,
144 Germany) and other solutions were autoclaved. Cells were incubated in a 250 mL baffled flask
145 at 30 °C and shaken at 200 rpm. Exponentially growing cells were harvested by centrifugation
146 (Sigma 3-18K centrifuge, Sigma-Aldrich, Seelze, Germany) at 5,000 *g* for 15 min at room
147 temperature, washed twice in fresh medium without glucose, and this inoculum was used to
148 inoculate microtiter plates or bioreactors. A 0.5 M stock solution of inducer was prepared by
149 solubilizing 3-methyl-benzoate (3-MB) (Sigma-Aldrich, St Louis, MO, USA) in 0.5 M NaOH.

150 **2.3 Batch culture in microtiter plate.** *P. putida* KT2440 CAP (pSEVA438_MBPeGFP) inoculum
151 was diluted to an optical density at 600 nm (OD_{600}) of 0.07 (Genesys 6 spectrophotometer,
152 Thermo, Carlsbad, CA, USA) in 5 mL M9 medium containing 3 g·L^{-1} glucose and 200 µg/mL
153 streptomycin and supplemented with 50 µL of different inducer concentrations (0, 0.5, 1, 2.5,
154 5, 10, 25, 50, 100, 250, 500, 1000 µM) prepared from a 0.5 M stock solution of 3-MB (Sigma-
155 Aldrich, St Louis, MO, USA) solubilized in a 0.5 M NaOH solution and filtered through a 0.2 μm
156 filter for sterilization (Minisart 0.2 µm syringe filter; Sartorius, Göttingen, Germany). These
157 dilutions were then inoculated (100 µL) in triplicate into a 96 well microtiter plate (Sarstedt,

158 Nümbrecht, Germany) and incubated at 30 °C in a plate reader (CLARIOstar^{Plus}, BMG Labtech,
159 Ortenberg, Germany). The optical density at 600 nm (OD_{600}) and fluorescence of GFP
160 (excitation wavelength, λex, 470 nm; emission wavelength 1, λem1, 515 nm),
161 autofluorescence (λex, 470 nm; λem, 580 nm) and *mCherry* (λex, 570 nm; λem, 620 nm) were
162 measured every 20 min for 48 h under continuous 200 rpm double orbital shaking. Three
163 independent biological replicates were analyzed.

164 **2.4 Batch culture in bioreactors.** *P. putida* KT2440 WT and *P. putida* CAP
165 (pSEVA438_MBPeGFP) were grown in a 500 mL bioreactor (my-Control, Applikon
166 Biotechnology INC, Sunnyvale, CA, USA) filled with 300 mL of M9 medium containing 4.0 $g \cdot L^{-1}$
167 NH_4Cl, 2.0 $g \cdot L^{-1}$ KH_2PO_4, 0.5 $g \cdot L^{-1}$ NaCl, 0.5 $g \cdot L^{-1}$ $MgSO_4$, 3.3 $mg \cdot L^{-1}$ $CaCl_2$, and 1 mL of the trace
168 element solution supplemented with 10 $g \cdot L^{-1}$ glucose. For flux analysis, ^{12}C-glucose was
169 replaced by a 10 $g \cdot L^{-1}$ mixture of 80 % (mol/mol) $^{13}C_1$-labeled glucose and 20 % (mol/mol) U-
170 $^{13}C_6$-labeled glucose (with a ^{13}C purity of 99 %; Eurisotop, Saint Aubin, France). The pH was
171 maintained at 7.0 ± 0.1 by automatically adding 14% (g/g) ammonia (VWR, Fontenay-sous-
172 Bois, France) or 10 % (g/g) phosphoric acid (PanReac AppliChem, Barcelona, Spain) and the
173 temperature was set to 30 °C. Adequate aeration of the culture was achieved by automatically
174 controlling the stirrer speed and the gas flow to maintain > 30 % oxygen saturation.
175 Streptomycin (200 µg/mL) was added to the *P. putida* CAP (pSEVA438_MBPeGFP) culture. The
176 inducer for protein production was added before cell inoculation, at 10 µM or 1 mM from a
177 0.5 M stock solution of 3-MB (Sigma-Aldrich, St Louis, MO, USA) solubilized in 0.5 M NaOH.
178 Foaming was avoided by manually adding 50 µL of antifoam 204 (Sigma-Aldrich, St Louis, MO,
179 USA) before inoculation and when required during growth. The bioreactor was inoculated to
180 an OD_{600} of 0.15. Depending on the culture time, 1.0 to 2.5 mL of culture were withdrawn
181 from the bioreactor every 0.5 to 1 h to monitor the OD_{600}, fluorescence, and protein and

182 metabolite contents of the culture. Cell dry weight (CDW) was determined by filtering 5 mL of
183 cells grown in M9 supplemented with glucose at OD_{600} 1.0, 1.5 and 2.0 on preweighed
184 membrane filters (Sartorius 0.2 µm, 47 mm, Goettingen, Germany) under vacuum filtration.
185 The filters were then washed with a 0.9 % NaCl solution, incubated at 80 °C and weighed every
186 24 h until a constant weight was reached. Under our laboratory conditions, the OD_{600} CDW
187 correlation for *P. putida* was CDW [$g \cdot L^{-1}$] = 0.57 ± 0.01 × OD_{600}.

188 **2.5 Fluorescence data processing.** The green fluorescence specifically emitted by eGFP was
189 measured in relative light units (RLU_{GFP}) using a procedure similar to the one described by
190 Lichten et al. (2014). The autofluorescence signal emitted by growing cells was estimated by
191 determining the ratio (r_a) of fluorescence at λem = 515 nm – specific to eGFP fluorescence
192 signals – and 580 nm (non-specific to eGFP fluorescence signals) of a *P. putida* KT2440 WT
193 culture grown in microtiter plate, yielding a $r_a = RLU_{515}/RLU_{580}$ = 2.479 (R^2=0.999; Figure S1A
194 supplementary data). Next, based on these data, the fluorescence emitted at 515 nm and at
195 580 nm by a culture of *P. putida* CAP (pSEVA438_MBPeGFP) was measured at each time point
196 and the autofluorescence was subtracted from the level of green fluorescence, yielding the
197 amount of fluorescence specific to the heterologous protein, $RLU_{GFP} = RLU_{515} - r_a x RLU_{580}$,
198 (Lichten et al., 2014).The overlap between the autofluorescence signal of the cells and the
199 fluorescence emitted by mCherry at 620 nm was negligible.

200 **2.6 Purification of heterologous protein**. The heterologous protein MBPeGFP was purified
201 using NEBExpress Ni spin columns (NEB**,** Ipswich, MA, USA) according to manufacturer
202 recommendations. Briefly, 50 mL of *P. putida* CAP (pSEVA438_MBPeGFP) culture induced with
203 1 mM of 3-MB (Sigma-Aldrich, St Louis, MO, USA) were extracted from a bioreactor at OD_{600}
204 of 2.25, harvested at 5,000 *g* for 15 min, and stored at -80 °C until further analysis. Frozen cell

205 pellets were resuspended in 4 mL of IMAC buffer (NEB**,** Ipswich, MA, USA) on ice and dispersed
206 using an ultrasonic disruptor (Sonics, VibraCell^{TM}, Newtown, CT, USA) in 9 sonication cycles
207 (20 s ON, 30 s OFF; power amplitude, 20 %) with a pause of 60 s in between. Cell debris was
208 removed by centrifugation (15 min at 16,100 *g*). Protein purification was then carried out
209 following the manufacturer's protocol. After adding 200 µL of elution buffer containing 50 mM
210 imidazole, the concentration of MBPeGFP was measured with a bicinchoninic acid (BCA) assay
211 using bovine serum albumin (BSA) dilutions ranging from 0 to 206.25 µg/mL to establish a
212 standard curve (Figure S1B). Purified MBPeGFP was two-fold serially diluted. BSA standard
213 and purified protein (25 µL) were each added in triplicate to a microtiter plate (Sarstedt,
214 Nümbrecht, Germany) and 200 µL of a 50:1 mixture of BCA and copper(II) sulfate solutions
215 (Sigma-Aldrich, St Louis, MO, USA) was added to each well containing a sample. The plate was
216 incubated for 30 min at 37 °C, then left to cool at room temperature for 5 min before
217 absorbance was measured at 562 nm with a plate reader (CLARIOstar^{Plus}, BMG Labtech,
218 Ortenberg, Germany). The final concentration of purified protein was 1076 µg/mL. This stock
219 solution was then diluted (at concentrations of 175, 150, 125, 100, 75, 50 µg/mL) and mixed
220 with 4X Laemmli buffer (Biorad, Hercules, CA, USA) containing 1 % β-mercaptoethanol for SDS-
221 PAGE calibration, as detailed below (Figure S1C and S1D).

222 **2.7 Heterologous protein quantification by SDS-PAGE and fluorescence correlation factor.**
223 Bioreactor culture samples (60 µL) were extracted at an OD_{600} of 1 to 4, diluted to an OD_{600} of
224 1, mixed with 4X Laemmli buffer (Biorad, Hercules, CA, USA) containing 1 % β-
225 mercaptoethanol and stored at −20 °C until analysis. After denaturation for 5 min at 95 °C, 8
226 µL of cellular extract and dilutions of purified protein (at 175, 150, 125, 100, 75, 50 µg/mL)
227 were loaded onto a 12.5 % SDS-PAGE gel and separated at 160 V for 70 min in a mini-protean
228 tetra cell (Biorad, Hercules, CA, USA) using Tris-glycine-SDS running buffer. The gels were

229 washed once with distilled water and stained with InstantBlue® Coomassie Protein Stain
230 (Abcam, Cambridge, UK). The gels were viewed using a ChemiDOC XRS molecular imager
231 (Biorad, Hercules, CA, USA) (Figure S1C) and the images were analyzed using Image Lab v6.0.1
232 (Biorad, Hercules, CA, USA). Brightness and contrast were adjusted automatically using the
233 software. Lanes and bands were identified manually. The lane profile tool was used to quantify
234 the peak area that corresponded as precisely as possible to the protein band. The resulting
235 calibration curve for MBPeGFP (Figure S1D) was used to estimate its concentration in the
236 samples (Figure S1E). A correlation factor between the amount of green fluorescence
237 ($RLU_{MBPeGFP}$) emitted by the sample and the protein concentration was calculated from the
238 slope of the curve (Fluo factor 7.25×10^{-9} - 0.0007, $R^2 = 0.954$). This was used to convert the
239 levels of green fluorescence measured in other samples into MBPeGFP protein
240 concentrations.

241 **2.8 Quantification of extracellular metabolites by NMR.**

242 Glucose, gluconate and 2-KG were identified and quantified by nuclear magnetic resonance
243 (NMR). Culture samples (1 mL) were collected every 0.5 to 1 h during growth, centrifuged at
244 14,500 *g* for 3 min, and the supernatants were stored at −20 °C until analysis. The supernatants
245 (180 µL) were mixed with 20 µL of an internal standard consisting of 10 mM deuterated
246 trimethylsilylpropanoic acid (TSP-d4) diluted in D_2O. Proton NMR spectra were recorded on
247 an Avance III 500-MHz spectrometer equipped with a 5-mm z-gradient TXI (^1H, ^{13}C, ^{31}P) probe
248 (Brucker, Rheinstatten, Germany). Quantitative ^1H NMR analysis was performed at 286 K,
249 using a zgpr30 sequence with a recycle delay of 10 s, and presaturation at 4.7 ppm for water
250 suppression. Thirty-two scans were accumulated (32k data points with a spectral width of 10
251 ppm) after 4 dummy scans. Inverse gated ^{13}C decoupling was used for samples containing ^{13}C-

252 Glucose to ensure the spectra were quantitative. The zgigpr sequence was used with ^{13}C
253 decoupling during ^{1}H acquisition (396 ms), a recycle delay of 10 s, and presaturation at 4.7
254 ppm for water suppression. Thirty-two scans were accumulated (8k data points with a spectral
255 width of 20 ppm). The spectra were processed using Topspin 3.1 (Bruker, Rheinstatten,
256 Germany). The reported results are the average values obtained from at least three biological
257 replicates.

258 **2.9 Calculation of Growth Rates and Extracellular Fluxes**

259 Growth rates and extracellular metabolite fluxes were determined in the exponential growth
260 phase from the time courses of biomass, glucose, gluconate and 2-KG concentrations, as
261 measured by NMR. All calculations were performed using PhysioFit 1.0.2 (Peiro et al., 2019)
262 (https://github.com/MetaSys-LISBP/PhysioFit) from culture profiles obtained with unlabeled
263 or ^{13}C-labeled glucose (Figure S2). MBPeGFP and mCherry production rates ($q_{MBPeGFP}$ and
264 $q_{mcherry}$) were calculated by multiplying the respective yields by the growth rate.

265 **2.10 ^{13}C-labeled samples and quantitative isotopic analysis.**

266 Samples of culture medium (100 µL) for quantitative isotopic analyses and ^{13}C-metabolic flux
267 analyses were collected during the exponential growth phase (between OD_{600} 2 and 4) from
268 culture grown on ^{13}C-glucose. The samples were plunged and vigorously mixed in 2 mL of
269 methanol/acetonitrile/H_2O (4:4:2) precooled at -20 °C, incubated for 2 h at -20 °C, evaporated
270 overnight in a SpeedVac (SC110A SpeedVac Plus, ThermoSavant, Waltham, MA, USA) and
271 stored at -80 °C until IC-MS analysis. The cell extracts were then resuspended in 100 µL
272 deionized water, and centrifuged at 14,500 *g* for 10 min at 4 °C to remove cell debris. Mass
273 fractions of intracellular metabolites were quantified using an ion chromatograph (IC; Thermo
274 Scientific Dionex ICS- 50001 system; Dionex, Sunnyvale, CA, United States) coupled to an LTQ

275 Orbitrap mass spectrometer (Thermo Fisher Scientific, Waltham, MA, United States) equipped
276 with a heated electrospray ionization (HESI) probe. Fourier transform mass spectra were
277 recorded in full-scan negative ion mode at a resolution of 60,000 at m/z = 400. The ion
278 chromatography and mass spectrometry experiments are described in greater detail
279 elsewhere (Vogeleer and Létisse, 2022). In total, three samples were analyzed for each of
280 three independent biological replicates.

281 Isotopologues were quantified from 11 metabolic intermediates covering the central
282 metabolism (6-phosphogluconate, glucose 6-phosphate, fructose 6-phosphate, fructose 1,6-
283 bisphosphate, 2/3-phosphoglycerate, phosphoenolpyruvate, ribose 5-phosphate,
284 sedoheptulose 7-phosphate, citrate/isocitrate, malate and succinate). The mass fractions
285 were corrected for naturally occurring isotopes, using IsoCor 2.2.0 ((Millard et al., 2019),
286 https://github.com/MetaSys-LISBP/IsoCor) and high resolution spectra (60,000 at m/z = 400),
287 with corrections for the natural abundance and isotopic purity (99 %) of the tracer element.

288 **2.11 ^{13}C-Metabolic flux analyses**

289 ^{13}C metabolic fluxes were calculated using the software influx_s (Sokol et al., 2012), based on
290 a flux model that included the mass balances and carbon atom transitions of *P. putida*'s main
291 central metabolic pathways (Kohlstedt and Wittmann, 2019; Nikel et al., 2015): glucose
292 uptake, glycolysis (EMP), pentose phosphate pathway (PPP), ED pathway, tricarboxylic acid
293 cycle (TCA), anaplerotic reactions, and gluconate and 2-KG secretion. Following Kohlstedt and
294 Wittmann (2019), the flux through the Kdgk reaction was fixed at 4.9 % of the flux through the
295 Gntk reaction. Precursor requirements for biomass synthesis were estimated based on the
296 composition of the biomass (van Duuren et al., 2013) and growth rates. Similarly, precursor
297 requirements for the synthesis of heterologous protein were estimated from the protein

298 sequence and from protein production rates. Intracellular fluxes were estimated by fitting i)
299 extracellular fluxes (glucose uptake, and gluconate, 2-KG, biomass and protein production)
300 and ii) the ^{13}C-labelling patterns of intracellular metabolites measured by IC-MS. A chi-square
301 statistical test was used to assess the goodness-of-fit (based on 95 % confidence intervals) for
302 each condition. For comparison, the estimated fluxes were then normalized to the rate of
303 substrate uptake, set to 100. For each condition, the mean fluxes and the corresponding
304 standard deviations were determined from three independent biological replicates. The
305 isotopic data and metabolic fluxes for each independent biological replicate are given in Table
306 S2 in the supplementary material. All model files and flux calculation results are available at
307 https://github.com/MetaSys-LISBP/pseudomonas_metabolic_burden.

308 **2.12 Calculation of carbon, redox and energy balances**

309 The carbon balance was determined by calculating the proportion of carbon converted from
310 glucose to biomass, gluconate, 2-KG, CO_2 and heterologous protein during the exponential
311 phase as outlined in the Results section. The amounts of biomass, gluconate, 2-KG and
312 heterologous protein produced were quantified as described above. The amount of CO_2
313 produced during the exponential phase was calculated from the percentage concentrations
314 of CO_2 and N_2 measured in the gas output using a Dycor ProLine Process mass spectrometer
315 (Ametek, Berwyn, PA, USA). The biomass formula was assumed to be $C_1H_{1.52}O_{0.41}N_{0.27}P_{0.02}S_{0.01}$
316 (van Duuren et al., 2013).

317 NADPH production and consumption fluxes were estimated by summing the fluxes through
318 all reactions producing or consuming NADPH along with NADPH fluxes for the synthesis of
319 biomass (anabolism) and heterologous protein. The apparent excess of NADPH may be
320 converted to NADH through the activities of pyridine nucleotide transhydrogenases (SthA and

321 PntAB) (Nikel et al., 2016b), as shown in previous work (Kohlstedt and Wittmann, 2019).
322 Similarly, ATP production *via* substrate-level phosphorylation was calculated by summing the
323 fluxes of ATP-producing reactions and subtracting the fluxes of ATP-consuming reactions. ATP
324 produced *via* oxidative phosphorylation was inferred from the production rates of NADH,
325 $FADH_2$ and $FMNH_2$, assuming P/O ratios of of 1.875 for the conversion of NADH and $PQQH_2$
326 into ATP and a P/O ratio of 1.0 for the conversion of $FADH_2$ (Nikel et al., 2015). ATP demand
327 was calculated by summing the requirements for anabolism, non-growth-associated
328 maintenance (van Duuren et al., 2013), and for the biosynthesis of the heterologous protein,
329 assuming 5 ATP equivalents per amino acid residue added (Garett and Grisham, 1999).

330 **3. Results**

331 **3.1 Characterization of the metabolic burden in *P. putida***

332 To characterize the physiological impact of the metabolic burden due to heterologous protein
333 production in *P. putida* KT2440, we introduced a fluorescent protein under the control of a
334 constitutive promoter into the *att* site in the chromosome as a proxy for the biosynthetic
335 capacity of *P. putida* cells. We chose the mCherry fluorescent protein controlled by the *lacIp*
336 promotor from the *E. coli lac*-operon, which is not regulated when isolated from its original
337 genomic environment. The amount of mCherry produced during heterologous protein
338 production was taken to be representative of the availability of cellular resources and served
339 as a proxy for the biosynthetic capacity of the cells (Ceroni et al., 2015). The reasoning behind
340 is that the amount of fluorescent protein produced from the non-regulated promoter should
341 resemble the amount of protein produced from the native constitutive promoters in the
342 genome. Thus, it can be understood as a stand-in for the availability of cellular resources, such
343 as RNAP, Ribosomes, tRNAs, or amino acids.

344 The eGFP labeled protein chosen to impose a metabolic burden was introduced into *P. putida*
345 KT2440 cells on a plasmid under the control of an inducible promoter (Figure 2A). The eGFP
346 domain was fused to the C-terminus of MBP, forming a 623-amino-acid fusion protein,
347 MBPeGFP (Figure 2B). The advantages of MBPeGFP for this study were that the fluorescence
348 emitted by eGFP could be used to estimate protein yields during growth, while the MBP
349 domain increased solubility and limited aggregation (Raran-Kurussi et al., 2015). To facilitate
350 purification, a His-tag was added to the C-terminal part of the eGFP domain (sequence is
351 available in supplementary data). The MBPeGFP encoding gene was integrated into
352 pSEVA438, under the control of a XylS/Pm expression system induced by 3-MB.

353 The associated metabolic burden was quantified in terms of the growth, biosynthetic capacity
354 and heterologous protein production of *P. putida* CAP (pSEVA438_MBPeGFP) cultures in
355 microtiter plates. These small-scale experiments demonstrated that both the mCherry
356 production and the maintenance of the pSEVA438 plasmid did not impose a noticeable
357 metabolic burden (Figure S3). We rather assumed that these processes consume part of the
358 metabolic leeway. Next, the production of MBPeGFP was modulated by exposing the cells to
359 various concentrations of 3-MB inducer, from 0 to 1000 µM.

360 Four types of behavior can be distinguished in these data. First, at very low 3-MB
361 concentrations (< 0.5 µM), the small amounts of MBPeGFP produced did not represent a
362 metabolic burden since there was no impact on *P. putida* growth or biosynthetic capacity
363 (mCherry production). However, some MBPeGFP production was observed even in the
364 absence of inducer, indicating that as reported previously (Balzer et al., 2013), the XylS/Pm
365 expression system is slightly leaky. The growth rate (μ_{max}) was 0.57 ± 0.02 h^{-1} (Figure 2C), as
366 reported in the literature for this strain when grown on glucose (Kohlstedt and Wittmann,

367 2019; Kozaeva et al., 2021). Second, exposure to between 0.5 and 10 µM 3-MB was associated
368 with a dramatic reduction in μ_{max} from 0.57 ± 0.02 h^{-1} to 0.15 ± 0.02 h^{-1}, and decreased
369 mCherry production (Figure 2D). This relationship between growth rate and biosynthetic
370 capacity is in agreement with Ceroni et al.'s findings in *E. coli* (2015) . The MBPeGFP production
371 rate remained constant, meaning that the decrease in cell growth did not directly translate
372 into a higher heterologous protein production rate (Figure 2E). Under these conditions,
373 resource sharing is detrimental to cell growth with no clear benefit in terms of protein
374 production. From 10 to 250 µM 3-MB, the MBPeGFP production rate gradually increased while
375 cell growth and mCherry production remained constant. The MBPeGFP production rate at 250
376 µM 3-MB was twice what it was at 10 µM 3-MB. Here too, the rates of cell growth and protein
377 production did not directly counterbalance each other, indicating that the coordination of
378 these processes is more complex than a simple sharing of cellular resources. Finally, exposing
379 the cells to more than 250 µM 3-MB did not increase the MBPeGFP production rate and had
380 no additional impact on their growth rate or biosynthetic capacity.

381 Having observed that exposing *P. putida* CAP (pSEVA438_MBPeGFP) to various concentrations
382 of inducer generated different levels of metabolic burden, we explored how the central
383 metabolism of the host copes with *low* (without inducer), *medium* (10 µM 3-MB), and *high*
384 (1000 µM 3-MB) degrees of metabolic burden. We chose the *P. putida* KT2440 wild-type strain
385 as a reference in this study, as there was no major difference in either growth rate or capacity
386 - where applicable - between WT and CAP strains harboring or not the empty plasmid (Figure
387 S3). On the other hand, quantitative data on metabolic fluxes are available for this strain in
388 the literature, which allows us to compare and validate our methodology for analyzing
389 metabolic fluxes (Kohlstedt and Wittmann, 2019).

390 **3.2 Quantitative analysis of *P. putida* physiology during heterologous protein production.**

391 Cell cultures were scaled-up from micro-titer plates to bioreactors so that key environmental
392 parameters (pH, dissolved oxygen tension (DOT), temperature, agitation, *etc.*) could be
393 adjusted precisely. *P. putida* CAP (pSEVA438_MBPeGFP) was cultivated in minimal medium
394 supplemented with 10 $g \cdot L^{-1}$ glucose as sole carbon source and containing either none, 10 µM
395 or 1000 µM 3-MB. Cells were grown in the presence of unlabeled or ^{13}C-labeled glucose
396 (Figure S2) and growth parameters and carbon balances (Table 1 and Figure 3) were
397 determined from the growth profiles. Intracellular fluxes were determined from the cultures
398 supplemented with ^{13}C-labeled glucose (see paragraph 3.5).

399 In the absence of inducer, *P. putida* CAP (pSEVA438_MBPeGFP) grew at the same rate (0.58 ±
400 0.02 h^{-1}) in the bioreactor as in the microtiter plate (Figure 2) and as the WT strain in the
401 bioreactor (Table1). This value is also similar to those reported in the literature for growth on
402 glucose (Kohlstedt and Wittmann, 2019). In the presence of 10 or 1000 µM 3-MB, the growth
403 rates in the exponential phase were half (0.29 ± 0.02 h^{-1}) and one third (0.19 ± 0.04 h^{-1}) of the
404 non-induced value, respectively. As observed in microtiter plates, the production rate of
405 mCherry also decreased, by 20% and 50%, respectively.

406 Under non-induced conditions, MBPeGFP represented an estimated 0.47± 0.1 % of the total
407 CDW, confirming the slight leakiness of the XylS/Pm expression system. In the presence of 10
408 µM and 1000 µM inducer, the production rate of MBPeGFP increased by factors of almost 4
409 and 10, respectively, leading to heterologous protein yields of 3.49 ± 1.1 % and 13.6 ± 2.0 %
410 of the total CDW (Table 1).

411 These results show that the chosen induction conditions had the expected effects, namely a
412 *low* metabolic burden in the absence of induction, and *medium* and *high* burdens with 10 and
413 1000 µM 3-MB, respectively.

414 **3.3 Protein production modifies the periplasmic metabolism**

415 The burden imposed by the synthetic expression system for maintenance and protein
416 production leads to profound modifications of the central metabolism (Wittmann et al., 2007).
417 To investigate the metabolic rearrangements occurring in *P. putida* in response to
418 heterologous protein production, the dynamic profiles of extracellular metabolites in the
419 culture media of WT and CAP (pSEVA438_MBPeGFP) *P. putida* strains were quantified by
420 NMR.

421 *P. putida* has been observed to produce gluconate and small amounts of 2-KG during
422 exponential growth on glucose, with concentrations peaking at 5 mM and 0.2 mM,
423 respectively (Figure S2), and both compounds subsequently being co-consumed with glucose
424 (Nikel et al., 2015). In the absence of inducer, a similar profile was observed here for
425 gluconate, while the 2-KG concentration dropped and approached the limit of detection
426 (Figure S2). The concentrations of both compounds reached much higher levels in the
427 presence of inducer, with the concentration of 2-KG peaking at 2 and 4 mM in the presence
428 of 10 and 1000 µM 3-MB, respectively. No other metabolites were found to accumulate in
429 these experiments.

430 The rates of glucose consumption (q_{Glc}), gluconate and 2-KG production (q_{Gnt} and q_{2KG}), and
431 mCherry and MBPeGFP production ($q_{mcherry}$, q_{GFP}) were determined during the exponential
432 growth phase based on the concentrations of biomass and extracellular metabolites and on
433 protein fluorescence. The fact that these rates were constant throughout the exponential

434 growth phase indicates that the cells had reached a steady state (Table 1 and Figure S4). Under
435 low MBPeGFP production conditions, the rates of glucose consumption (6.9 $mmol \cdot g^{-1} \cdot h^{-1}$ ±
436 0.5) and gluconate production (0.81 ± 0.18 $mmol \cdot g^{-1} \cdot h^{-1}$) were similar to those calculated for
437 the WT strain (Table 1) (Kohlstedt and Wittmann, 2019). Under medium and high MBPeGFP
438 production conditions, glucose consumption decreased to 4.2 ± 0.3 $mmol \cdot g^{-1} \cdot h^{-1}$ in the
439 presence of 10 µM 3-MB and 3.4 ± 0.3 $mmol \cdot g^{-1} \cdot h^{-1}$ at 1000 µM 3-MB, while 2-KG production
440 was close to 0.2 $mmol \cdot g^{-1} \cdot h^{-1}$ under both conditions (Table 1). CO_2 production was also lower
441 under these conditions than in the WT strain.

442 These results indicate that heterologous protein production caused a marked slowdown of
443 metabolic activity in *P. putida* CAP (pSEVA438_MBPeGFP), as reflected in particular by the
444 lower rate of glucose consumption. More surprising is the sharp change in periplasmic
445 metabolism evidenced by the accumulation of 2-KG. To the best of our knowledge, this
446 phenomenon has never previously been reported in *P. putid*a, but it is similar to the acetate
447 overaccumulation observed under recombinant protein production conditions in *E. coli* (San
448 et al., 1994; Ying Lin and Neubauer, 2000).

449 **3.4 Heterologous protein production consumes very little carbon but profoundly alters the**
450 **distribution of carbon usage in *P. putida***

451 The carbon balance was calculated for each condition by summing the amounts of carbon
452 used to produce biomass, gluconate, 2-KG, CO_2 and heterologous protein (Figure 3). These
453 compounds accounted for nearly 100 % of carbon usage in each case (WT: 98 ± 1 %,
454 uninduced: 99 ± 2 %, 10 µM: 100 ± 4 %, 1000 µM: 98 ± 8 %), confirming that no other carbon
455 molecules were produced in significant amounts. Under low MBPeGFP production conditions,
456 the proportions of carbon used for biomass, gluconate, CO_2 and 2-KG production were similar

457 to those observed for the WT strain. The proportion of carbon used for biomass production
458 decreased to 0.46 ± 0.01 Cmol/Cmol and 0.39 ± 0.07 Cmol/Cmol under medium and high
459 protein production conditions, respectively, while the proportion of carbon diverted to
460 gluconate decreased by a factor of 1.6 and 2.8, respectively, and the fraction used for 2-KG
461 production increased significantly to 5 ± 2 % of total carbon usage at 10 µM 3-MB and 9 ± 4 %
462 1000 µM 3-MB. Remarkably, the total amount of carbon converted into gluconate and 2-KG
463 was constant across all studied conditions.

464 The proportion of carbon used for MBPeGFP production was negligible in the absence of
465 inducer, and was just 0.03 ± 0.01 Cmol/Cmol and 0.04 ± 0.02 Cmol/Cmol in the presence of 10
466 and 1000 µM 3-MB, respectively. However, the amount of carbon excreted as CO_2 by the cell
467 increased from 0.31 ± 0.05 Cmol/Cmol without inducer to 0.38 ± 0.02 Cmol/Cmol in the
468 presence of 10 µM 3-MB and 0.44 ± 0.05 Cmol/Cmol with 1000 µM 3-MB (Figure 3). In other
469 words, under conditions of significant heterologous protein production, part of the carbon
470 normally used for biomass was completely oxidized into CO_2. Therefore, although production
471 of the heterologous protein only accounted for a small percentage of the total carbon
472 consumed, it had a profound impact on cellular metabolism.

473 **3.5 Metabolic flux analyses reveal metabolic rearrangements in the central metabolism of**
474 ***P. putida***

475 We employed ^{13}C metabolic flux analysis to measure the alterations in the central metabolism
476 of *P. putida* in response to heterologous protein production. To minimize the impact of culture
477 history, we quantified ^{13}C incorporation in central metabolites that have a faster turnover rate
478 compared to the end products of the carbon metabolism. Data was collected from the cultures
479 grown in the presence of ^{13}C-labeled glucose (Figure S2).

480 **3.5.1 Metabolic flux map for *P. putida* WT**

481 We first compared the central metabolic flux distribution measured in WT *P. putida* KT2440
482 (Figure 4) with those based on LC- or GC-MS based ^{13}C metabolic flux analyses reported in the
483 literature (Nikel et al., 2015; Kohlstedt and Wittmann, 2019). Similarly to previous reports, we
484 found that glucose was mainly oxidized in the periplasm into gluconate (91 %) by glucose
485 dehydrogenase (Gcd) and to a lesser extent (5 %) into 2-KG by gluconate dehydrogenase
486 (Gad), with a significant (> 10 %) gluconate excretion into the culture supernatant. Most of the
487 gluconate (76 %) was phosphorylated into 6-phosphogluconate (6PG). At this metabolic node,
488 the carbon flux through the 2-KG bypass was 4 %. 6PG was mainly channeled into the ED
489 pathway *via* 2-keto-3-deoxy-6-phosphogluconate (2-KDPG), cleaved into glyceraldehyde-3-
490 phosphate (G3P) and pyruvate. G3P was mainly driven toward the low EMP pathway, where
491 it converged with 2-KDPG breakdown at the pyruvate node. Approximatively 20 % of G3P was
492 directed toward the EDEMP cycle. Despite this flux, glucose was mainly oxidated in the
493 periplasm, where the oxidative flux was 6 times higher than in the cytoplasm. The flux
494 channeled through the EDEMP cycle is however essential as it increases the NADPH reducing
495 power and ensures the supply of precursors (R5P, E4P, F6P) required for anabolism. Finally,
496 pyruvate was mainly driven toward the TCA cycle, with no significant flux through the
497 glyoxylate shunt. The concerted action of pyruvate dehydrogenase (Pdh) and pyruvate
498 carboxylase (Pyc) fuels the TCA cycle while replenishing the supply for anabolic needs. The flux
499 through malic enzyme (Mae) was remarkably high, contributing approximately one quarter of
500 the total influx into the pyruvate pool.

501 **3.5.2 Metabolic flux map for *P. putida* CAP (pSEVA438_MBPeGFP).**

502 Next, we examined the metabolic flux distributions in the central metabolism of *P. putida* CAP
503 (pSEVA438_MBPeGFP) under different degrees of metabolic burden.

504 As mentioned above, *P. putida* CAP (pSEVA438_MBPeGFP) produced small amounts of
505 heterologous protein even in the absence of inducer, exploiting only a part of its free capacity.
506 The flux distribution in the absence of inducer was similar to the one determined for the WT
507 strain (Figure 4B), indicating that using a small amount of *P. putida*'s free capacity only has a
508 negligible effect on the carbon flux distribution. In other words, this metabolic leeway can be
509 exploited to produce exogenous compounds such as proteins without affecting the cellular
510 machinery. Increasing this free capacity would therefore appear to be a viable strategy to
511 increase the amount of heterologous protein that can be produced without imposing a
512 metabolic burden. For example, removing 4.3 % of dispensable genes from *P. putida*'s genome
513 (including genes encoding for flagellar motility and genome stability) has been observed to
514 improve heterologous protein yields by 40 % (Lieder et al., 2015).

515 In contrast, the central metabolic flux distribution of *P. putida* CAP (pSEVA438_MBPeGFP) was
516 profoundly altered under medium and high metabolic burdens. First, periplasmic gluconate
517 oxidation into 2-KG by FAD-dependent Gad increased up to 2-fold without any significant
518 change either in gluconate oxidation through the ED pathway *via* gluconate kinase (GntK) or
519 *via* 2-KG bypass (Figure 4B). The increased flux through Gad was compensated by a 2-fold
520 decrease in excreted gluconate and by significant excretion of 2-KG. Therefore, this metabolic
521 reshuffling resulted mainly in increased production of $FADH_2$ through Gad flux.

522 Second, whereas the flux through the EDEMP cycle tended to decrease under increased
523 MBPeGFP production, the flux through the other pathways of the central metabolism
524 increased, particularly through the endergonic subset of the EMP pathway and in the TCA

525 cycle. The fluxes through phosphoglycerate kinase (Pgk), phosphopyruvate hydratase (Eno)
526 and pyruvate kinase (Pyk) increased by respectively 10 %, 12 % and 7 % under medium
527 MBPeGFP production compared with the low production condition, and by 22 %, 26 % and 50
528 % respectively at high MBPeGFP production (Figure 4A and 4B). The fluxes through the TCA
529 cycle dehydrogenases (isocitrate dehydrogenase (Idh), α-ketoglutarate dehydrogenase
530 (AkgdH), succinate dehydrogenase (Sdh) and to a lesser extent malate dehydrogenase (Mdh))
531 increased by roughly 15% and 25% under medium and high MBPeGFP production conditions
532 relative to the baseline level. In addition, the glyoxylate cycle was not activated by protein
533 production.

534 This analysis of metabolic fluxes shows that the production of the heterologous protein
535 MBPeGFP leads to a reshuffling of *P. putida*'s central carbon metabolism, with carbon fluxes
536 redirected toward the oxidative catabolic pathway. This presumably provides the extra
537 chemical and redox energy required to synthesize the heterologous protein and counter the
538 corresponding stress while still satisfying basic housekeeping needs.

539 **3.6 *P. putida* generates an apparent excess of ATP under heterologous protein production**
540 **conditions**

541 The rearrangement of central carbon fluxes for heterologous protein production point to an
542 important adjustment of energy metabolism. We therefore calculated redox and ATP fluxes
543 from the measured flux distributions as described in the Materials and Methods section.

544 In agreement with previous studies (Kohlstedt and Wittmann, 2019; Nikel et al., 2015), our
545 data indicate that *P. putida* WT generates a catabolic excess of NADPH (Figure 5A). Isocitrate
546 dehydrogenase (Idh) supplies roughly half of the NADPH, and malic enzyme a third. The
547 oxidative branch of the PP pathway contributes very little, despite it being the main

548 contributor to NADPH production in other microorganisms, such as *E. coli* (Nicolas et al.,
549 2007). The apparent surplus of NADPH is converted into NADH *via* transhydrogenase activities
550 (PntAB and SthA). As expected in aerobic growth, ATP is overwhelmingly produced by
551 oxidative phosphorylation, mainly for anabolic purposes (Figure 5B). Unlike NADPH, ATP-
552 production and consumption balance out (>93 %).

553 Compared to the WT strain, NADPH production fluxes were respectively 27 %, 45 % and 54 %
554 lower in the CAP (pSEVA438_MBPeGFP) strain under low, medium and high MBPeGFP
555 production conditions, respectively (Figure 5A). While the NADPH consumption flux was
556 similar to the WT strain's under low MBPeGFP production conditions, it was much lower under
557 medium and high MBPeGFP production. NADPH was mainly used for anabolism, and less than
558 one-fifth (8.6%) of the total NADPH consumed was used for heterologous protein synthesis
559 under high protein production conditions. As in the WT strain, NADPH production exceeded
560 the cellular demand, with the excess amount accounting for a large proportion of total NADPH
561 production under medium and high MBPeGFP production conditions (43 ± 11 % and 53 ± 5 %
562 respectively). Excessive NADPH production during heterologous protein production has also
563 been reported for other microorganisms (Daniels et al., 2018; Driouch et al., 2012; Nocon et
564 al., 2016; Toya et al., 2014). Similar to the WT strain, the apparent surplus of NADPH was
565 converted into NADH by transhydrogenase.

566 Regarding energy metabolism, low MBPeGFP production did not have an obvious impact on
567 production and consumption fluxes in the CAP (pSEVA438_MBPeGFP) strain (Figure 5B). In
568 contrast, under medium and high protein production conditions, ATP production and
569 consumption fluxes were reduced by 36 % and 39 %, respectively, compared to the WT strain,
570 while the contributions of oxidative phosphorylation and anabolic demand to the ATP balance

571 remained close to the levels estimated in the WT strain. Remarkably, the amount of ATP used
572 for heterologous protein production was very low, even under high induction. As observed for
573 NADPH, a large apparent surplus of ATP was generated upon medium and high MBPeGFP
574 production, representing respectively 25 % and 40 % of the total ATP consumed. This large
575 apparent excess probably covered unquantified energy usages in protein biosynthesis, such
576 as protein folding, as well as cellular adaptations to the stresses associated with protein
577 overproduction (Hoffmann and Rinas, 2004).

578 **3.7 Metabolic control analysis of heterologous protein production**

579 We then aimed to quantify the extent of control exerted by heterologous protein production
580 on metabolic fluxes using flux control coefficients (C_p^J), which quantify the degree of control
581 exerted by a given parameter *p,* here the protein production rate, on each flux *J*. Control
582 coefficients were calculated as the fractional change in the steady-state flux *J* in response to
583 a fractional change in *p* (Fell and Thomas, 1995; Heinrich and Rapoport, 1974; Kacser and
584 Burns, 1973):

585 $$C_p^J = \frac{\delta J}{J} \Big/ \frac{\delta p}{p} = \frac{\delta \ln J}{\delta \ln p}$$

586 If the C_p^J coefficients remain constant across different experiments in which *p* is modulated,
587 their value can be estimated by fitting a linear function to a *ln-ln* plot, whose slope is equal to
588 the control strength. Here, we used (steady-state) data collected for the various levels of
589 protein production (Figure 4 and Table S2) to estimate the control exerted by protein
590 production on carbon and energy fluxes. The C_p^J coefficients measure the sensitivity of the
591 system to both direct metabolic regulation (though thermodynamics and metabolite-enzyme

592 interactions), as well as to the indirect (hierarchical) action of signal transduction and gene
593 expression.

594 The degree of control exerted by the MBPeGFP production rate on carbon and energy fluxes
595 was investigated at the level of individual reactions and for more global processes such as
596 growth and ATP and NADPH formation. This analysis provided an overall picture of the cellular
597 processes affected by heterologous protein production (Figure 6). Among the analyzed fluxes,
598 a majority of fluxes (25 out of 40, accounting for 63 %) showed a significant correlation with
599 protein production ($r^2 > 0.5$, $p < 0.02$). This indicates that the control exerted on these
600 reactions remained stable across all MBPeGFP production conditions. The low r^2 values (high
601 p-values) obtained for the other fluxes may indicate an absence of control (*e.g.* Gnd) or reflect
602 more complex, nonlinear control patterns that cannot be captured by linear regression (*e.g.*
603 Ppc) (Figure S5).

604 Looking more closely at the control coefficients, MBPeGFP production exerted a negative
605 control on virtually all fluxes (with coefficients ranging from -0.17 to -0.99), in line with the
606 global decrease in fluxes observed in response to MBPeGFP production. This negative control
607 was observed for glucose uptake (C_p^{qGLC} = -0.30 ± 0.05, r^2 = 0.80, p = 5.10^{-4}), periplasmic
608 glucose oxidation (C_p^{gcd} = -0.59 ± 0.10, r^2 = 0.80, p = 5.10^{-4}), the ED pathway (C_p^{edd} = -0.62 ±
609 0.11, r^2 = 0.79, p = 6.10^{-4}), the EMP pathway (C_p^{pgk} = -0.52 ± 0.09, r^2 = 0.80, p = 5.10^{-4}; C_p^{fba} =
610 -0.99 ± 0.28, r^2 = 0.60, p = 8.10^{-3}), and the TCA cycle (C_p^{cs} = -0.53 ± 0.09, r^2 = 0.83, p = 3.10^{-4}).
611 Significant control was also observed on ATP fluxes ($C_p^{ATP_prod}$ = -0.20 ± 0.04, r^2 = 0.78, p =
612 8.10^{-4}), with similar levels of control on ATP production *via* oxidative phosphorylation and *via*
613 substrate phosphorylation, and on NADPH fluxes ($C_p^{NADPH_prod}$ = -0.17 ± 0.06, r^2 = 0.51, p =
614 0.02). The control on energy and redox fluxes was weaker (coefficients between -0.17 and -

615 0.19) than on carbon fluxes (coefficients between -0.30 and -0.99), indicating that in *P. putida*
616 CAP (pSEVA438_MBPeGFP), energy fluxes are less sensitive to heterologous protein
617 production than carbon fluxes are. These results also indicate that the fraction of glucose used
618 for energy production increased with the level of heterologous protein production. These
619 metabolic rearrangements were reflected in terms of cell physiology by a strong control on
620 the growth rate (C_p^{growth}= -0.46 ± 0.08; r^2 = 0.79, p = 5.10^{-4}).

621 These results offer a quantitative understanding of the impact of heterologous protein
622 production on *P. putida*'s metabolism. The level of control remained largely stable across the
623 three induction levels studied, indicating that all pathways responded smoothly to
624 heterologous protein production. The fact that the response of carbon fluxes was more
625 pronounced compared to energy fluxes highlights the flexibility of the central carbon
626 metabolism and the robustness of the energy metabolism in *P. putida*.

627 **Conclusions**

628 In this study, we conducted a detailed quantitative analysis to examine how *P. putida* responds
629 to different degrees of metabolic burden caused by heterologous protein production. Our
630 results indicate that low levels of heterologous protein production do not require any
631 metabolic adaptation, because the extra demand does not exceed *P. putida*'s free capacity.
632 However, when this free capacity is exceeded, growth is progressively inhibited and a global
633 slowdown of metabolism is observed. Despite the relatively low (< 5%) carbon usage
634 associated with heterologous protein production, our study revealed significant
635 rearrangements in metabolic fluxes. These rearrangements indicate that even a small fraction
636 of carbon dedicated to protein production can have a profound impact on the overall
637 metabolic network of *P. putida.* As revealed by metabolic control analysis, heterologous

638 protein production exerts a tighter control on carbon fluxes than on energy fluxes, suggesting
639 that the flexible nature of *P. putida*'s central metabolic network is solicited to maintain energy
640 production (Martin-Pascual et al., 2021; Tokic et al., 2020; Zobel et al., 2016). The metabolic
641 flux response indicates a smooth, progressive decoupling of anabolism from catabolism, with
642 energy production increasing far beyond the expected energy demands for protein
643 biosynthesis. Similar behaviour was observed in other micro-organisms (Daniels et al., 2018;
644 Driouch et al., 2012; Nocon et al., 2016; Toya et al., 2014), highlighting the genericity of
645 microbial response to metabolic burdens. The reconfiguration of metabolic fluxes leads to an
646 energy surplus well beyond what is necessary for growth and the production of heterologous
647 proteins. This apparent surplus encompasses energy needs for various processes difficult to
648 quantify and often underestimated. These include cellular maintenance, replication and
649 expression of plasmids, the translation and folding of the heterologous protein, as well as the
650 energy required to cope with the various other stresses induced by heterologous protein
651 production. These stresses remain to be elucidated and warrant further investigation.

652 From a metabolic engineering perspective, this study showed that the expression of a very
653 simple genetic circuit consisting of an inducible protomer and one gene encoding the MBP
654 fused to eGFP, is accompanied by a drastic reduction in growth rate, which goes hand in hand
655 with reduced glucose uptake, and a more pronounced conversion of glucose to gluconate and
656 2-KG, which then leaves the cell. The rearrangement of the metabolic fluxes is also reflected
657 by less NADPH and ATP production. These findings could be a first starting point to streamline
658 *P. putida* towards a better production of heterologous proteins following the design-build-
659 test-learn (DBTL) cycle concept for metabolic engineering (Liu et al., 2015). In the design phase
660 genetic targets will be selected, in the build phase the manipulation of *P. putida* will take place,
661 which will then be characterized to obtain the data necessary to learn and predict parameters

662 that can be applied in the next DBTL round. Interesting candidates that could be tackled in the
663 first design phase is i) the improvement of glucose uptake by the introduction of an additional
664 transporter, *e. g.* the Glf transporter (Bujdoš et al., 2023), ii) the blockage of the periplasmic
665 glucose conversion to gluconate and 2-KG by deletion of *gcd* (Poblete-Castro et al., 2014) and,
666 iii) the enhancement of the EDEMP cycle in order to modulate NADPH production by targeting
667 the activity of *zwf* (Nikel et al., 2016a).

668 **5. Conflict of Interest**

669 The authors declare that the research was conducted in the absence of any commercial or
670 financial relationships that could be construed as a potential conflict of interest.

671 **6. Funding**

672 This work was supported by the Agence Nationale de la Recherche [grant number ANR-18-
673 CE92-0027-01] and the Deutsche Forschungsgemeinschaft (DFG) [Project number
674 406709163].

675 **7. Acknowledgments**

676 The authors thank MetaToul (Metabolomics & Fluxomics Facilities, Toulouse, France,
677 www.metatoul.fr) and its staff for technical support and access to the NMR facility. MetaToul
678 is part of the French National Infrastructure for Metabolomics and Fluxomics
679 (www.metabohub.fr), funded by the ANR (MetaboHUB-ANR-11-INBS-0010). Edern Cahoreau
680 is gratefully acknowledged for assistance with NMR spectroscopy. The French National
681 Research Agency (ANR) and the German Research Foundation (DFG) are acknowledged for
682 funding of the CHEAP project and the ANR for funding a post-doctoral fellowship to P.V.

8. References

Balzer, S., Kucharova, V., Megerle, J., Lale, R., Brautaset, T., Valla, S., 2013. A comparative analysis of the properties of regulated promoter systems commonly used for recombinant gene expression in Escherichia coli. Microbial Cell Factories 12, 26. https://doi.org/10.1186/1475-2859-12-26

Borkowski, O., Ceroni, F., Stan, G.-B., Ellis, T., 2016. Overloaded and stressed: whole-cell considerations for bacterial synthetic biology. Current Opinion in Microbiology, Antimicrobials. Microbial systems biology 33, 123–130. https://doi.org/10.1016/j.mib.2016.07.009

Bujdoš, D., Popelářová, B., Volke, D.C., Nikel, P.I., Sonnenschein, N., Dvořák, P., 2023. Engineering of Pseudomonas putida for accelerated co-utilization of glucose and cellobiose yields aerobic overproduction of pyruvate explained by an upgraded metabolic model. Metab Eng 75, 29–46. https://doi.org/10.1016/j.ymben.2022.10.011

Ceroni, F., Algar, R., Stan, G.-B., Ellis, T., 2015. Quantifying cellular capacity identifies gene expression designs with reduced burden. Nat Methods 12, 415–418. https://doi.org/10.1038/nmeth.3339

Choi, K.-H., Schweizer, H.P., 2006. mini-Tn7 insertion in bacteria with single attTn7 sites: example Pseudomonas aeruginosa. Nat Protoc 1, 153–161. https://doi.org/10.1038/nprot.2006.24

Chung, C.T., Niemela, S.L., Miller, R.H., 1989. One-step preparation of competent Escherichia coli: transformation and storage of bacterial cells in the same solution. Proc Natl Acad Sci U S A 86, 2172–2175. https://doi.org/10.1073/pnas.86.7.2172

Daniels, W., Bouvin, J., Busche, T., Rückert, C., Simoens, K., Karamanou, S., Van Mellaert, L., Friðjónsson, Ó.H., Nicolai, B., Economou, A., Kalinowski, J., Anné, J., Bernaerts, K., 2018. Transcriptomic and fluxomic changes in Streptomyces lividans producing heterologous protein. Microb Cell Fact 17, 198. https://doi.org/10.1186/s12934-018-1040-6

de Lorenzo, V., 2008. Systems biology approaches to bioremediation. Current Opinion in Biotechnology, Chemical biotechnology / Pharmaceutical biotechnology 19, 579–589. https://doi.org/10.1016/j.copbio.2008.10.004

de Lorenzo, V., Timmis, K.N., 1994. Analysis and construction of stable phenotypes in gram-negative bacteria with Tn5- and Tn10-derived minitransposons. Methods Enzymol 235, 386–405. https://doi.org/10.1016/0076-6879(94)35157-0

del Castillo, T., Ramos, J.L., Rodríguez-Herva, J.J., Fuhrer, T., Sauer, U., Duque, E., 2007. Convergent Peripheral Pathways Catalyze Initial Glucose Catabolism in Pseudomonas putida: Genomic and Flux Analysis. J. Bacteriol. 189, 5142. https://doi.org/10.1128/JB.00203-07

Driouch, H., Melzer, G., Wittmann, C., 2012. Integration of in vivo and in silico metabolic fluxes for improvement of recombinant protein production. Metab Eng 14, 47–58. https://doi.org/10.1016/j.ymben.2011.11.002

Fell, D.A., Thomas, S., 1995. Physiological control of metabolic flux: the requirement for multisite modulation. Biochem J 311 (Pt1), 35–39. https://doi.org/10.1042/bj3110035

727 Garett, H.R., Grisham, M., Charles, 1999. Biochemistry, 2nd edition. ed. Sanders College
728 Publication, Fort Worth.
729 Heinrich, R., Rapoport, T.A., 1974. A linear steady-state treatment of enzymatic chains.
730 General properties, control and effector strength. Eur J Biochem 42, 89–95.
731 https://doi.org/10.1111/j.1432-1033.1974.tb03318.x
732 Hoffmann, F., Rinas, U., 2004. Stress induced by recombinant protein production in
733 Escherichia coli. Adv. Biochem. Eng. Biotechnol. 89, 73–92.
734 https://doi.org/10.1007/b93994
735 Kacser, H., Burns, J.A., 1973. The control of flux. Symp Soc Exp Biol 27, 65–104.
736 Kim, J., Park, W., 2014. Oxidative stress response in Pseudomonas putida. Appl Microbiol
737 Biotechnol 98, 6933–6946. https://doi.org/10.1007/s00253-014-5883-4
738 Kohlstedt, M., Wittmann, C., 2019. GC-MS-based 13C metabolic flux analysis resolves the
739 parallel and cyclic glucose metabolism of Pseudomonas putida KT2440 and
740 Pseudomonas aeruginosa PAO1. Metab Eng 54, 35–53.
741 https://doi.org/10.1016/j.ymben.2019.01.008
742 Kozaeva, E., Volkova, S., Matos, M.R.A., Mezzina, M.P., Wulff, T., Volke, D.C., Nielsen, L.K.,
743 Nikel, P.I., 2021. Model-guided dynamic control of essential metabolic nodes boosts
744 acetyl-coenzyme A–dependent bioproduction in rewired Pseudomonas putida.
745 Metabolic Engineering 67, 373–386. https://doi.org/10.1016/j.ymben.2021.07.014
746 Lichten, C.A., White, R., Clark, I.B., Swain, P.S., 2014. Unmixing of fluorescence spectra to
747 resolve quantitative time-series measurements of gene expression in plate readers.
748 BMC Biotechnology 14, 11. https://doi.org/10.1186/1472-6750-14-11
749 Lieder, S., Nikel, P.I., de Lorenzo, V., Takors, R., 2015. Genome reduction boosts heterologous
750 gene expression in Pseudomonas putida. Microb Cell Fact 14.
751 https://doi.org/10.1186/s12934-015-0207-7
752 Liu, R., Bassalo, M.C., Zeitoun, R.I., Gill, R.T., 2015. Genome scale engineering techniques for
753 metabolic engineering. Metab Eng 32, 143–154.
754 https://doi.org/10.1016/j.ymben.2015.09.013
755 Martin-Pascual, M., Batianis, C., Bruinsma, L., Asin-Garcia, E., Garcia-Morales, L., Weusthuis,
756 R.A., van Kranenburg, R., Martins Dos Santos, V.A.P., 2021. A navigation guide of
757 synthetic biology tools for Pseudomonas putida. Biotechnol Adv 49, 107732.
758 https://doi.org/10.1016/j.biotechadv.2021.107732
759 Millard, P., Delépine, B., Guionnet, M., Heuillet, M., Bellvert, F., Létisse, F., 2019. IsoCor:
760 isotope correction for high-resolution MS labeling experiments. Bioinformatics 35,
761 4484–4487. https://doi.org/10.1093/bioinformatics/btz209
762 Miller, J.H., 1972. Experiments in Molecular Genetics. Cold Spring Harbor Laboratory.
763 Nicolas, C., Kiefer, P., Letisse, F., Krömer, J., Massou, S., Soucaille, P., Wittmann, C., Lindley,
764 N.D., Portais, J.-C., 2007. Response of the central metabolism of Escherichia coli to
765 modified expression of the gene encoding the glucose-6-phosphate dehydrogenase.
766 FEBS Lett 581, 3771–3776. https://doi.org/10.1016/j.febslet.2007.06.066
767 Nikel, P.I., Chavarría, M., Danchin, A., de Lorenzo, V., 2016a. From dirt to industrial
768 applications: Pseudomonas putida as a Synthetic Biology chassis for hosting harsh
769 biochemical reactions. Curr Opin Chem Biol 34, 20–29.
770 https://doi.org/10.1016/j.cbpa.2016.05.011
771 Nikel, P.I., Chavarría, M., Fuhrer, T., Sauer, U., de Lorenzo, V., 2015. Pseudomonas putida
772 KT2440 Strain Metabolizes Glucose through a Cycle Formed by Enzymes of the Entner-

773 Doudoroff, Embden-Meyerhof-Parnas, and Pentose Phosphate Pathways. J Biol Chem
774 290, 25920–25932. https://doi.org/10.1074/jbc.M115.687749
775 Nikel, P.I., de Lorenzo, V., 2018. Pseudomonas putida as a functional chassis for industrial
776 biocatalysis: From native biochemistry to trans-metabolism. Metabolic Engineering,
777 Metabolic Engineering Host Organism Special Issue 50, 142–155.
778 https://doi.org/10.1016/j.ymben.2018.05.005
779 Nikel, P.I., Martínez-García, E., de Lorenzo, V., 2014. Biotechnological domestication of
780 pseudomonads using synthetic biology. Nat Rev Microbiol 12, 368–379.
781 https://doi.org/10.1038/nrmicro3253
782 Nikel, P.I., Pérez-Pantoja, D., de Lorenzo, V., 2016b. Pyridine nucleotide transhydrogenases
783 enable redox balance of Pseudomonas putida during biodegradation of aromatic
784 compounds. Environmental Microbiology 18, 3565–3582.
785 https://doi.org/10.1111/1462-2920.13434
786 Nocon, J., Steiger, M., Mairinger, T., Hohlweg, J., Rußmayer, H., Hann, S., Gasser, B.,
787 Mattanovich, D., 2016. Increasing pentose phosphate pathway flux enhances
788 recombinant protein production in Pichia pastoris. Appl Microbiol Biotechnol 100,
789 5955–5963. https://doi.org/10.1007/s00253-016-7363-5
790 Oehler, S., 2009. Feedback Regulation of Lac Repressor Expression in Escherichia coli. J
791 Bacteriol 191, 5301–5303. https://doi.org/10.1128/JB.00427-09
792 Peiro, C., Millard, P., de Simone, A., Cahoreau, E., Peyriga, L., Enjalbert, B., Heux, S., 2019.
793 Chemical and Metabolic Controls on Dihydroxyacetone Metabolism Lead to
794 Suboptimal Growth of Escherichia coli. Appl Environ Microbiol 85, e00768-19.
795 https://doi.org/10.1128/AEM.00768-19
796 Poblete-Castro, I., Borrero-de Acuña, J.M., Nikel, P.I., Kohlstedt, M., Wittmann, C., 2017. Host
797 Organism: Pseudomonas putida, in: Industrial Biotechnology. John Wiley & Sons, Ltd,
798 pp. 299–326. https://doi.org/10.1002/9783527807796.ch8
799 Poblete-Castro, I., Rodriguez, A.L., Lam, C.M.C., Kessler, W., 2014. Improved production of
800 medium-chain-length polyhydroxyalkanoates in glucose-based fed-batch cultivations
801 of metabolically engineered Pseudomonas putida strains. J Microbiol Biotechnol 24,
802 59–69. https://doi.org/10.4014/jmb.1308.08052
803 Raran-Kurussi, S., Keefe, K., Waugh, D.S., 2015. Positional effects of fusion partners on the
804 yield and solubility of MBP fusion proteins. Protein Expr Purif 110, 159–164.
805 https://doi.org/10.1016/j.pep.2015.03.004
806 San, K.Y., Bennett, G.N., Aristidou, A.A., Chou, C.H., 1994. Strategies in high-level expression
807 of recombinant protein in Escherichia coli. Ann N Y Acad Sci 721, 257–267.
808 https://doi.org/10.1111/j.1749-6632.1994.tb47399.x
809 Sokol, S., Millard, P., Portais, J.-C., 2012. influx_s: increasing numerical stability and precision
810 for metabolic flux analysis in isotope labelling experiments. Bioinformatics 28, 687–
811 693. https://doi.org/10.1093/bioinformatics/btr716
812 Tokic, M., Hatzimanikatis, V., Miskovic, L., 2020. Large-scale kinetic metabolic models of
813 Pseudomonas putida KT2440 for consistent design of metabolic engineering
814 strategies. Biotechnology for Biofuels 13, 33. https://doi.org/10.1186/s13068-020-
815 1665-7
816 Toya, Y., Hirasawa, T., Morimoto, T., Masuda, K., Kageyama, Y., Ozaki, K., Ogasawara, N.,
817 Shimizu, H., 2014. 13C-metabolic flux analysis in heterologous cellulase production by
818 Bacillus subtilis genome-reduced strain. Journal of Biotechnology 179, 42–49.
819 https://doi.org/10.1016/j.jbiotec.2014.03.025

820 Udaondo, Z., Molina, L., Segura, A., Duque, E., Ramos, J.L., 2016. Analysis of the core genome
821 and pangenome of Pseudomonas putida. Environ Microbiol 18, 3268–3283.
822 https://doi.org/10.1111/1462-2920.13015
823 van Duuren, J.B., Puchałka, J., Mars, A.E., Bücker, R., Eggink, G., Wittmann, C., dos Santos,
824 V.A.M., 2013. Reconciling in vivo and in silico key biological parameters of
825 Pseudomonas putidaKT2440 during growth on glucose under carbon-limited
826 condition. BMC Biotechnology 13, 93. https://doi.org/10.1186/1472-6750-13-93
827 van Winden, W., Verheijen, P., Heijnen, S., 2001. Possible Pitfalls of Flux Calculations Based on
828 13C-Labeling. Metabolic Engineering 3, 151–162.
829 https://doi.org/10.1006/mben.2000.0174
830 Vicente, M., Cánovas, J.L., 1973. Glucolysis in Pseudomonas putida: Physiological Role of
831 Alternative Routes from the Analysis of Defective Mutants. J Bacteriol 116, 908–914.
832 https://doi.org/10.1128/jb.116.2.908-914.1973
833 Vogeleer, P., Létisse, F., 2022. Dynamic Metabolic Response to (p)ppGpp Accumulation in
834 Pseudomonas putida. Front Microbiol 13, 872749.
835 https://doi.org/10.3389/fmicb.2022.872749
836 Volke, D.C., Calero, P., Nikel, P.I., 2020. Pseudomonas putida. Trends in Microbiology 28, 512–
837 513. https://doi.org/10.1016/j.tim.2020.02.015
838 Weimer, A., Kohlstedt, M., Volke, D.C., Nikel, P.I., Wittmann, C., 2020. Industrial biotechnology
839 of Pseudomonas putida: advances and prospects. Appl Microbiol Biotechnol 104,
840 7745–7766. https://doi.org/10.1007/s00253-020-10811-9
841 Wittmann, C., Weber, J., Betiku, E., Kromer, J., Bohm, D., Rinas, U., 2007. Response of fluxome
842 and metabolome to temperature-induced recombinant protein synthesis in
843 Escherichia coli. J Biotechnol 132, 375–84.
844 https://doi.org/10.1016/j.jbiotec.2007.07.495
845 Ying Lin, H., Neubauer, P., 2000. Influence of controlled glucose oscillations on a fed-batch
846 process of recombinant Escherichia coli. Journal of Biotechnology 79, 27–37.
847 https://doi.org/10.1016/S0168-1656(00)00217-0
848 Zobel, S., Benedetti, I., Eisenbach, L., de Lorenzo, V., Wierckx, N., Blank, L.M., 2015. Tn7-Based
849 Device for Calibrated Heterologous Gene Expression in Pseudomonas putida. ACS
850 Synth. Biol. 4, 1341–1351. https://doi.org/10.1021/acssynbio.5b00058
851 Zobel, S., Kuepper, J., Ebert, B., Wierckx, N., Blank, L.M., 2016. Metabolic response of
852 Pseudomonas putida to increased NADH regeneration rates. Eng Life Sci 17, 47–57.
853 https://doi.org/10.1002/elsc.201600072
854

855 **9. Figure legends**

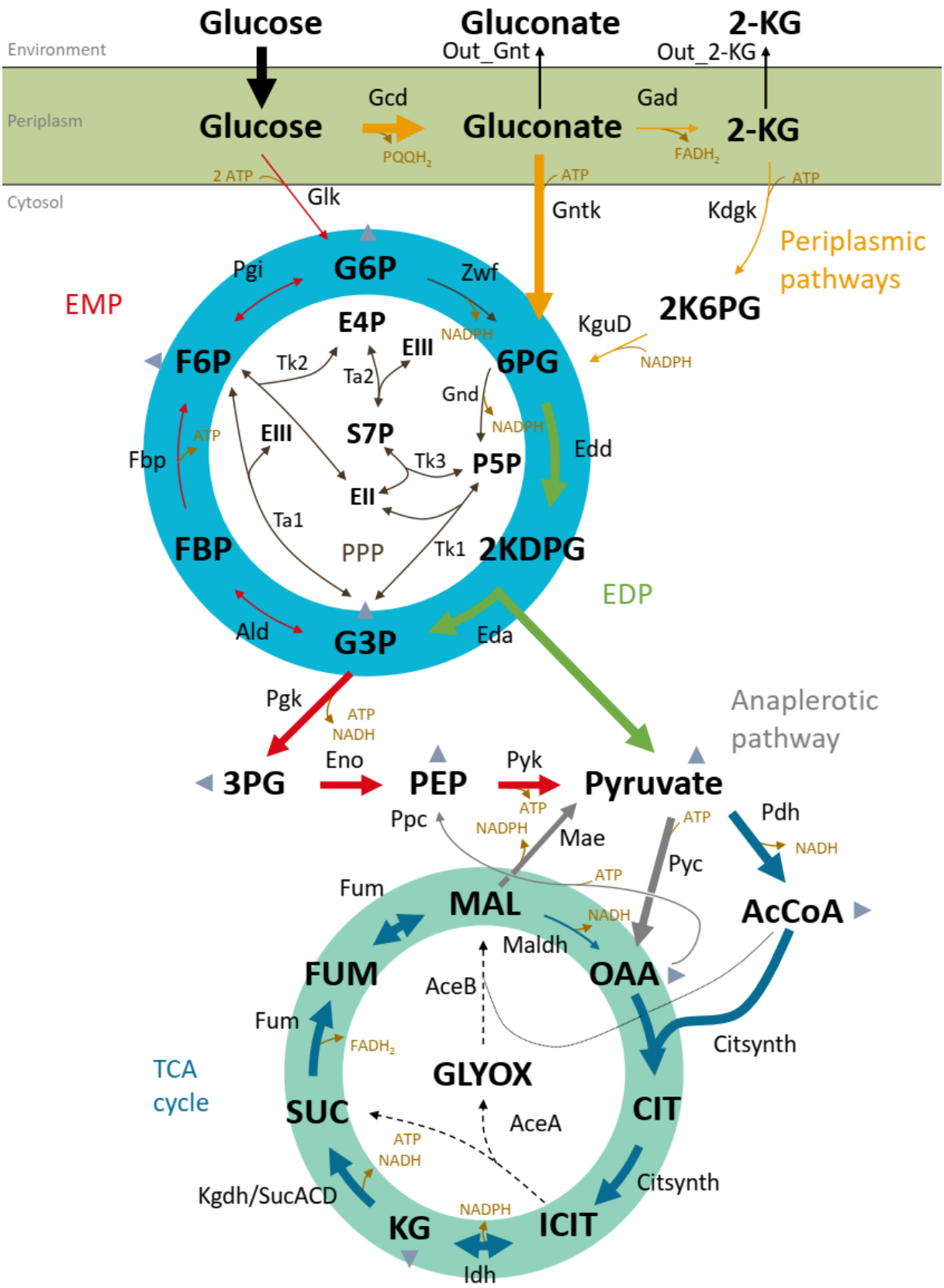

856

857 **Fig 1. Metabolic pathway of *P. putida* KT2440's central metabolism**. The EDEMP pathway is
858 circled in turquoise and the TCA cycle in water-green. Biomass precursors are indicated by
859 grey triangles. Arrow sizes reflect the intracellular carbon flux of glucose-grown cells relative
860 to the glucose uptake rate (set to 100 %) determined by Kohlstedt and Wittmann (Kohlstedt
861 and Wittmann, 2019). EII and EIII represent the C_2 and C_3 fragment pools, respectively, bound
862 to transketolase and transaldolase, and transferred to an aldose acceptor as described by
863 Kleijn et al. (2005). Reaction names and equations are provided in the supplemental data
864 (Table S1).

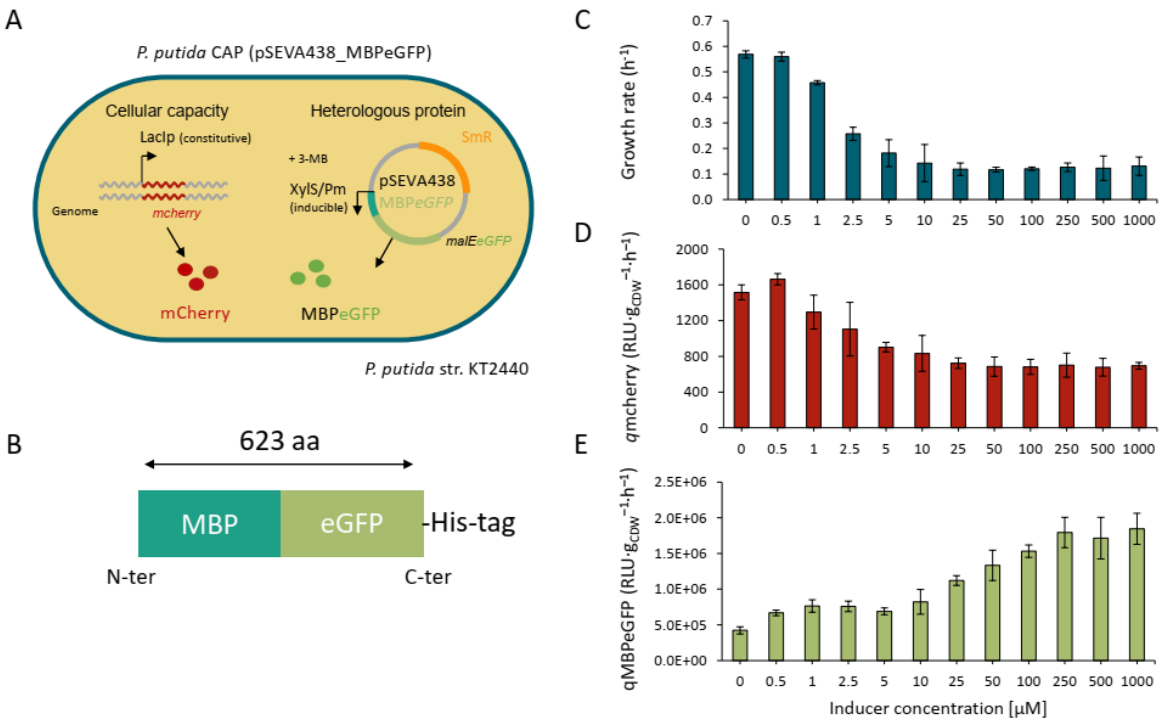

865

866 **Fig. 2. Physiological response of *P. putida* CAP (pSEVA438_MBPeGFP) to heterologous**
867 **protein production.** Schematic representation of the engineered *P. putida* strain with a red
868 fluorescent protein gene (*mCherry*) integrated into the chromosome to monitor biosynthetic
869 capacity and the green fluorescent fusion protein MBPeGFP encoded on a
870 pSEVA438_*MBPeGFP* plasmid (A). Schematic representation of the MBPeGFP fusion protein

871 with an N-terminal maltose binding protein (MBP) domain, the eGFP domain and a C-terminal
872 His-tag sequence (B). Growth rate (C), mCherry production rate (D) and MBPeGFP production
873 rate (E) of *P. putida* CAP (pSEVA438_MBPeGFP) cultivated with different inducer
874 concentrations. Results are averages from at least 3 biological replicates. 3-MB: 3-methyl-
875 benzoate.

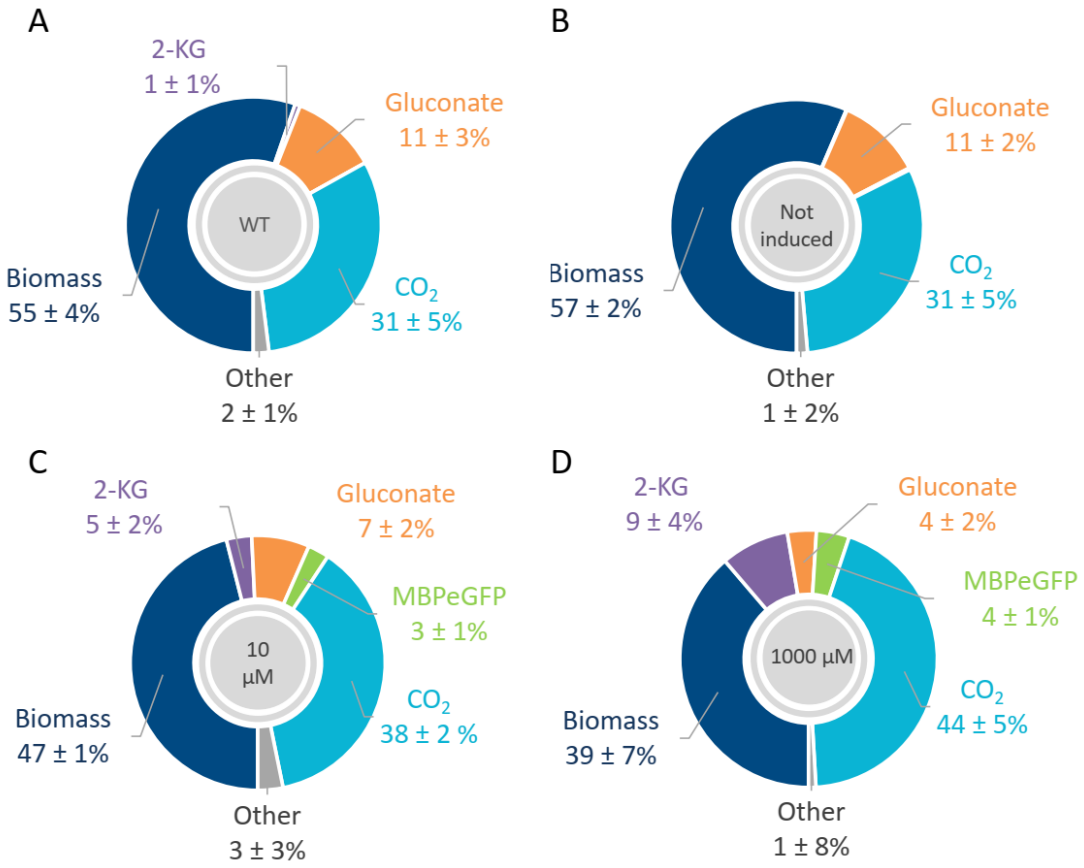

876

877 **Fig. 3: Carbon balance of glucose-grown *P. putida* KT2440 WT (A) and *P. putida* CAP**
878 **(pSEVA438_MBPeGFP) under low (B), medium (C) and high (D) heterologous protein**
879 **production conditions.** Carbon balances were calculated from the concentrations measured
880 in the media over exponential growth phase, highlighted in blue in Figure S2. Values represent
881 the mean ± standard deviation of three biological replicates for WT strain and four biological
882 replicates for CAP (pSEVA438_MBPeGFP) strain.

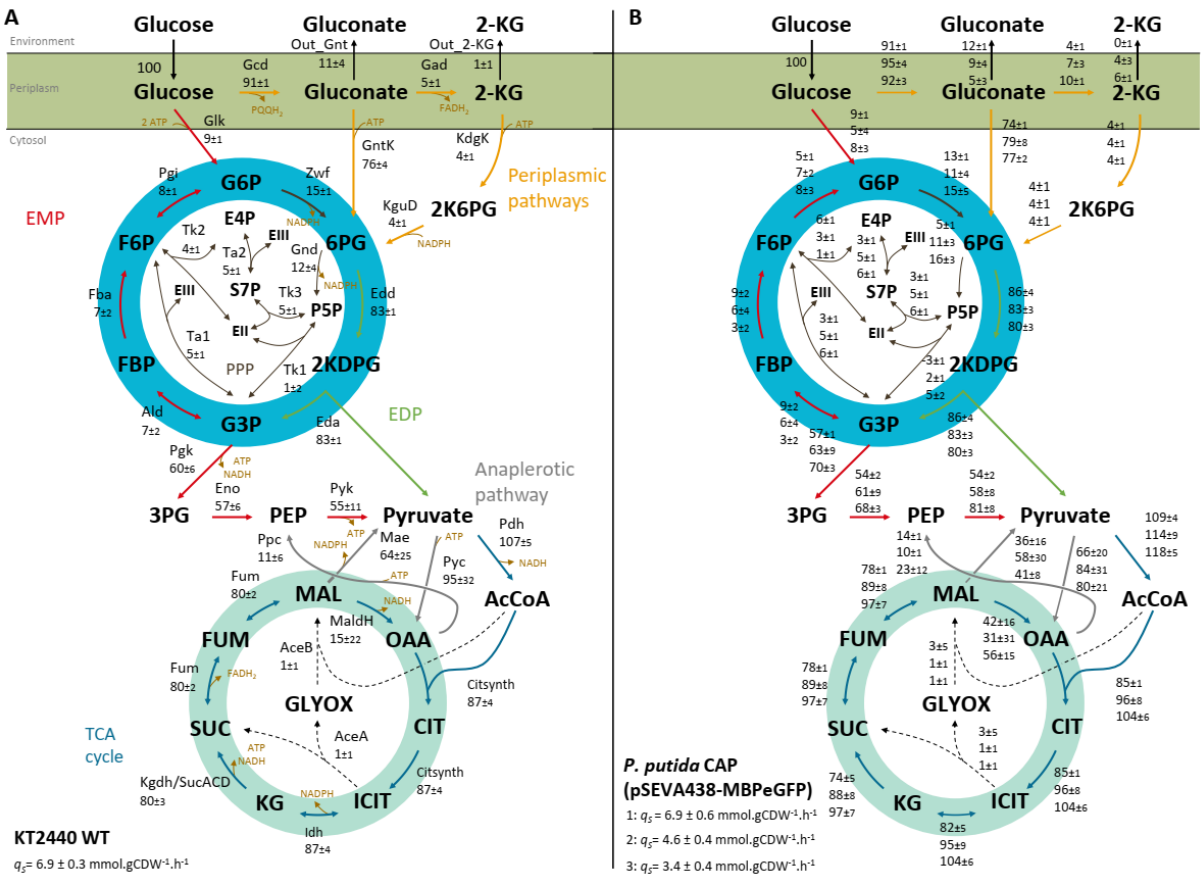

Fig. 4 Relative carbon flux distributions of KT2440 WT (A) and *P. putida* CAP (pSEVA438_MBPeGFP) (B) grown on glucose with or without 3-MB. All flux values are normalized to the specific glucose uptake rate of each condition, which was set to 100. Values represent the mean ± standard deviation of two biological replicates for the WT strain (A) and 3 biological replicates for the CAP (pSEVA438_MBPeGFP) strain (B). In panel B, the flux values correspond from top to bottom to: low (without inducer), medium (10 µM 3-MB), and high (1000 µM 3-MB) heterologous protein production conditions. Reaction names and equations are provided in the supplemental data (Table S1).

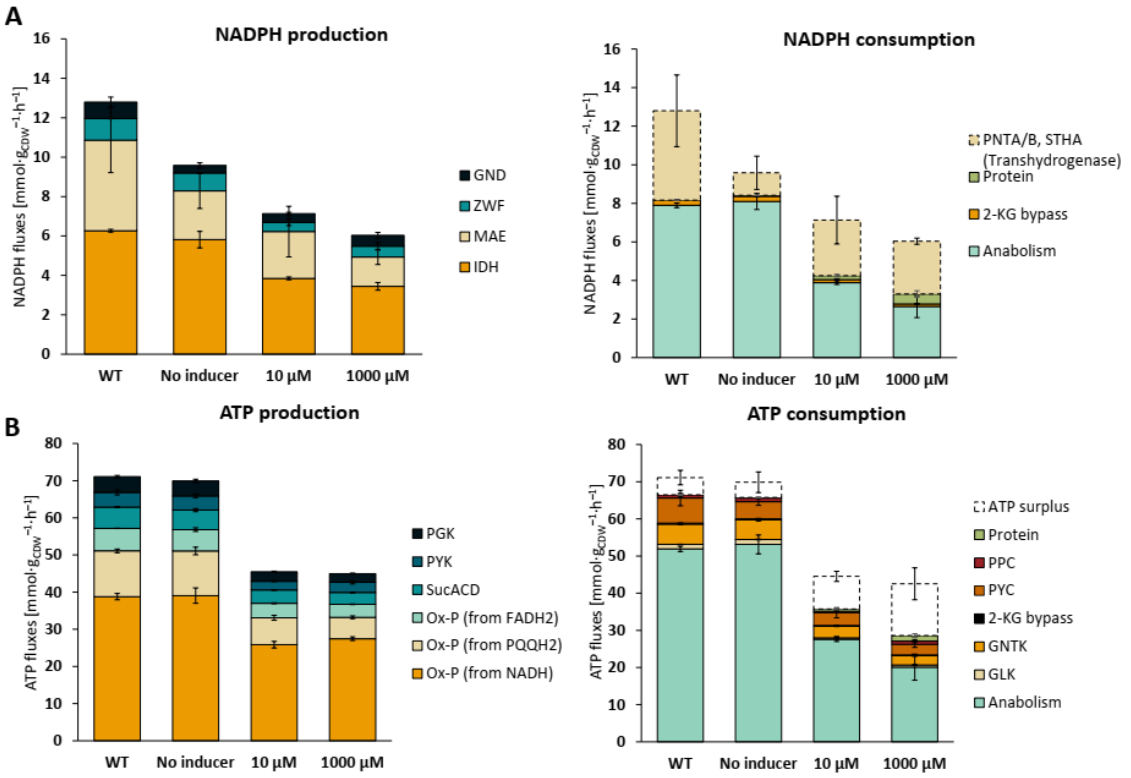

Fig. 5. Redox and energy fluxes of *P. putida* KT2440 WT and *P. putida* CAP (pSEVA438_MBPeGFP) grown on glucose with or without 3-MB. The absolute fluxes ($mmol \cdot g_{CDW}^{-1} \cdot h^{-1}$) related to the production and consumption of NADPH (A) and ATP (B) were determined from the carbon fluxes shown in Figure 4. Results are averages from 2 biological replicates for the WT strain and 3 biological replicates for the CAP (pSEVA438_MBPeGFP) strain; error bars represent standard deviations. Abbreviations: Gnd: 6-phosphogluconate dehydrogenase; Zwf: Glucose-6-P 1-dehydrogenase; Mae: malic enzyme; Idh: isocitrate deshydrogenase; Pgk: phosphoglycerate kinase; Pyk: pyruvate kinase; SucACD: succinyl CoA synthetase; Ox-P: oxidative phosphorylation; 2-KG bypass: 2-ketogluconate bypass; Ppc: phosphoenolpyruvate carboxylase; Pyc: pyruvate carboxylase; Gntk: gluconate kinase; Glk: Glucokinase.

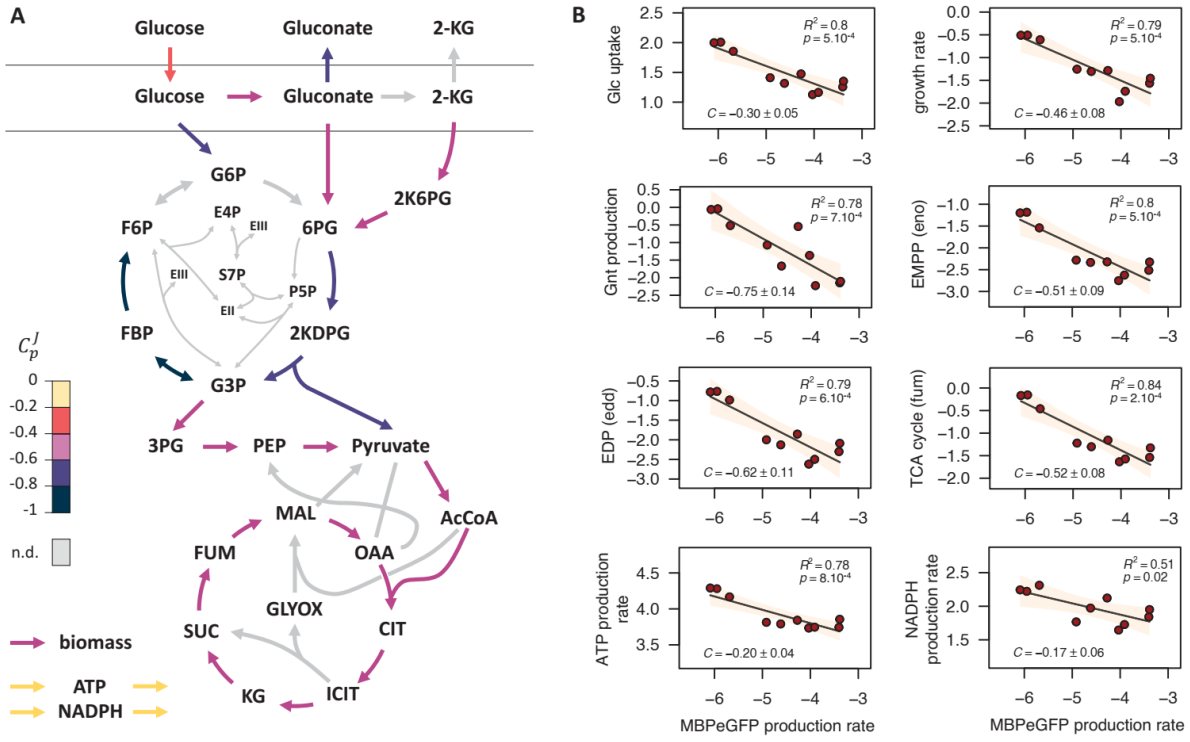

904

905 **Fig. 6. Control exerted on *P. putida*'s carbon and energy metabolism by heterologous protein**

906 **production.** Overview of the flux control coefficients (A). Control coefficients determined for

907 carbon and energy fluxes through the main pathways (glucose uptake, EMPP, EDP, TCA cycle,

908 ATP and NADPH production, and growth) (B), where dots represent experimental flux values

909 (expressed on a logarithmic scale), lines represent the best linear fits, and shaded areas

910 correspond to 95 % confidence intervals on the fits. Coefficients that could not be determined

911 reliably for some reactions are marked *n.d.*

912

913 **10. Table legends**

914 **Table 1**: **Growth parameters of glucose-grown *P. putida* KT2440 WT and *P. putida* CAP (pS**

915 **EVA438_MBPeGFP) for different inducer concentrations.**

Parameter	**WT strain (n=3)[b]**	***P. putida* CAP (pSEVA438-MBPeGFP) (n=4)[b]**		
3-methyl-benzoate (µM)	0	0	10 µM	1000 µM
μ_{max} **[(h^{-1})]**	0.58 ± 0.02	0.58 ± 0.03	0.29 ± 0.02	0.19 ± 0.04
$q_{mcherry}$ **(RLU · [g_{CDW} · h]$^{-1}$)**	ND[a]	1150 ± 101	928 ± 48	555 ± 112
$q_{MBPeGFP}$ **(mg · [g_{CDW} · h]$^{-1}$)**	ND[a]	2.8 ± 0.5	9.9 ± 2.9	26.2 ± 8.5
q_{CO2} **(mmol · [g_{CDW} · h]$^{-1}$)**	13.0 ± 1.9	12.5 ± 1.9	10.8 ± 1.3	9.0 ± 1.3
$Y_{X/S}$ **(g_X · mol^{-1})**	82.1 ± 6.8	84.4 ± 4.2	68.7 ± 3.9	55.0 ± 7.0
$Y_{MBPeGFP}$ **(mg · g_{CDW}^{-1})**	ND[a]	4.7 ± 1.0	34.9 ± 11.4	136.2 ± 19.8
q_{Glc} **(mmol · [g_{CDW} · h]$^{-1}$)**	7.0 ± 0.3	6.9 ± 0.5	4.2 ± 0.3	3.4 ± 0.3
q_{Gnt} **(mmol · [g_{CDW} · h]$^{-1}$)**	0.78 ± 0.22	0.81 ± 0.18	0.37 ± 0.16	0.15 ± 0.07
$q_{2\text{-}KG}$ **(mmol · [g_{CDW} · h]$^{-1}$)**	0.06 ± 0.01	0.02 ± 0.02	0.21 ± 0.03	0.22 ± 0.02

916 [a] Not detected

917 [b] The average values and standard errors of the means were calculated from the values

918 measured in *n* biological replicates.